Research paper

Comparison of Forest Canopy Height Derived Using Lidar Data and Aerial Photos

Jihn-Fa Jan[1,2)]

【Summary】

Forest composition and vertical structure provide essential information for understanding ecological states and processes in forest ecosystems. Recent development of lidar (light detection and ranging) technologies has led to applications of lidar in forest canopy structure investigations. The objective of this study was to develop a method to derive forest canopy height using a laser scanning instrument. Lidar data, acquired using a Leica ALS40 airborne laser scanner, of a deciduous forest were used in this study. In order to assess the capability of lidar for estimating canopy height of forest stands, a digital surface model derived from the local maximum of lidar data was compared to a digital surface model generated using a photogrammetric technique. In addition, forest canopy heights, represented by differences in the digital surface models and a 4-m digital elevation model, were calculated and compared for these 2 types of data. The results indicated that the canopy height generated from the lidar data was higher than that of the aerial photos, and the mean difference was about 0.22 m with a standard deviation of 2.59 m.

Key words: Lidar, photogrammetry, digital surface model, digital elevation model, forest canopy height.

Jan JF. 2005. Comparison of forest canopy height derived using lidar data and aerial photos. Taiwan J For Sci 20(1):13-27.

研究報告

應用空載雷射掃描資料與航空照片獲取林分高度之比較

詹進發[1,2)]

摘　要

森林之組成與垂直結構提供了重要的資訊，有助於了解森林生態系之生態狀態與過程，近年來空載雷射掃描技術的發展，促進了應用空載雷射掃描於調查森林植被結構之研究。本研究之目的為發展應用雷射掃描儀獲取林分高度之方法，使用之資料為利用Leica ALS40掃描闊葉樹林所產生的資料。為了評估空載雷射掃描用於估測林分之植被高度的能力，本研究由空載雷射掃描資料之區域極大值萃取出林分數值表面模型，並將其與航測方法所產生的林分數值表面模型做比較。此外，以林分數值表面

[1)] Department of Land Economics, National Chengchi University, 64, Sec. 2, Zhi-nan Road, Taipei 11605, Taiwan. 國立政治大學地政學系，11605台北市指南路二段64號。

[2)] Corresponding author. 通訊作者。

Received June 2004, Accepted December 2004. 2004年6月送審 2004年12月通過。

模型與一四公尺解析力之數值地形模型之差推估林分植被高度，並比較由空載雷射掃描與航測兩種資料所產生之林分高度。研究結果顯示，由空載雷射掃描資料所估測之林分高度略大於由航測所產生之林分高度，其高度差之平均值為0.22 m，標準差為2.59 m。

關鍵詞：空載雷射掃描、航空測量、數值表面模型、數值地形模型、林分高度。

詹進發。2005。應用空載雷射掃描資料與航空照片獲取林分高度之比較。台灣林業科學20(1):13-27。

INTRODUCTION

Forest ecosystem management depends on a wide variety of qualitative and quantitative information spanning different spatial and temporal scales. Obtaining the required information through ground investigations is often not feasible, because it is too costly in terms of time, manpower, and resources. Consequently, remote sensing techniques have successfully been used in many applications, such as forest resource inventories (Haara and Haarala 2002, Brown de Colstoun et al. 2003, Wulder et al. 2004), habitat monitoring (Imhoff et al. 1997), landscape change detection (Ulbricht and Heckendorff 1998, Franklin 2001), natural hazard investigations (Utkin et al. 2002), assessments of damages caused by insects and diseases (Franklin 2001, Skakun et al. 2003), leaf area index and forest biomass estimation (Fassnacht et al. 1996, Wulder 1998, Lim and Treitz 2002), and ecosystem modeling (Viedma et al. 1997).

The forest's composition and vertical structure provide essential information for understanding ecological states and processes in forest ecosystems (Lefsky et al. 2002). Most remote sensing systems, despite having remarkable capabilities to characterize the horizontal organization of vegetation canopies due to advances in remote sensing technologies which have improved the spectral and spatial resolutions in recent years, do not provide direct measurements of forest height characteristics (Lefsky et al. 2002, Lim et al. 2003). Similar to radar (radio detection and ranging), lidar (light detection and ranging) is a very advanced, active remote sensing technique which uses laser light as the energy source. Lidar obtains measurements at a very high density, therefore it provides excellent horizontal resolution. Additionally, lidar has the capability of recording multiple return pulses of the initial laser energy. Classification of these return pulses yields both the ground elevation and non-ground elevation, which allows direct measurements of the heights of buildings and vegetation (Wehr and Lohr 1999). Recent developments in lidar technologies have led to applications of lidar to various kinds of forest ecosystem research such as forest canopy structure investigations (Drake et al. 2002, Hudak et al. 2002, Lefsky et al. 2002, Lim et al. 2003), biomass estimation (Lefsky et al. 1999, Lefsky et al. 2002, Lim and Treitz 2002), and forest fire detection (Utkin et al. 2002).

This research utilized an airborne lidar system for obtaining data about the Yangmingshan National Park area, northern Taiwan, and techniques for deriving a digital surface model (DSM) using lidar data were investigated. In addition, the lidar measurements were used to measure forest canopy heights by subtracting a digital elevation model (DEM) from the DSM. To assess the capability of lidar in estimating forest canopy height, the height measurements derived from the lidar data were compared to the results generated from photogrammetric procedures.

MATERIALS AND METHODS

Study area

The study area for this research is located within the Yangmingshan National Park, a very popular recreation area in the vicinity of the Taipei City, northern Taiwan. The elevation of the park ranges from 200 to 1,120 m with a total area of 11,455 ha. Established in 1985, the park features unique volcanic landscapes and numerous species of plants and animals. Vegetation within the park can roughly be grouped into 3 categories: aquatic plants, grasslands, and forestlands. There are more than 1,200 plant species, of which several are endemic. Silvergrass (*Miscanthus floridules*) and arrow bamboo (*Sinobambusa kunishii*) often grow in grasslands, and the forest canopy is primarily composed of broad-leaf tree species, among which the Lauraceae family is dominant, including the red nanmu (*Machilus thunbergii*) and the large-leaved nanmu (*Machilus kusanoi*). Consisting of a cluster of more than 20 volcanoes, the park is famous for its outstanding natural beauty, geological features, and abundant hot spring resources (Anonymous 2004).

Data

1. Lidar data

The lidar data for the study area were acquired using a Leica ALS40 airborne laser scanner mounted on an airplane on 14 April 2002. The sensor was equipped with an aircraft position and orientation system (POS), which recorded the aircraft's position and attitude information using a global positioning system (GPS) receiver and an inertial measurement unit (IMU). The POS data were processed using proprietary software to generate World Geodetic System 1984 (WGS84) ground coordinates of all the reflected laser pulses (Leica Geosystems 2002). Furthermore, the data were transformed from WGS84 to a local coordinate system, and subsequently a filtering process was performed to separate ground points from non-ground points. The flight parameters and the number of points in the lidar datasets provided by the vendor are shown in Table 1.

2. Aerial photographs

Aerial photographs taken on 12 March 2002 were acquired for this study. The aerial photographs were taken along 2 flight lines using normal color film with a nominal scale of approximately 1:22,000. In total, 9 aerial photographs were acquired for this study. Characteristics of the aerial photographs and flight parameters are given in Table 2.

Table 1. Flight parameters and number of points in the lidar dataset

Flying height	1200~2200 m above ground level
FOV	35°
Scan rates	29.4 Hz
Pulse rates	38 kHz
All points	22,734,756 (812 MB)
Surface points	15,892,054 (580 MB)
Ground points	1,686,303 (60 MB)

Table 2. Characteristics of the aerial photographs

Topography	hilly
Nominal scale	1:22,000
Acquisition date	12 March 2002
Camera	Zeiss RMKTOP15
Focal length	152.818 mm
Film format	230×230 mm
Film material	Color
Flight altitude	4100 m ASL
Scanning resolution	1200 dpi
Nominal ground resolution	46.2 cm

3. Satellite images

QuickBird satellite images, provided by DigitalGlobe (Longmont, Colorado, U.S.A.), acquired on 15 December 2002 were obtained for the study area. The spatial resolution for the panchromatic and multispectral images were 0.7 and 2.8 m, respectively. Technical data of the satellite images are listed in Table 3. The satellite images were used for interpretation of land cover types in order to select appropriate sample areas for further investigation.

Table 3. Technical data of the QuickBird satellite images

Orbit altitude	450 km
Swath width	16.5 × 16.5 km at nadir
Digitization	11 bits
Resolution	Pan: 61 cm (nadir) to 72 cm (25° off-nadir) MS: 2.44 m (nadir) to 2.88 m (25° off-nadir)
Image bands	Pan: 450 ~ 900 nm Blue: 450 ~ 520 nm Green: 520 ~ 600 nm Red: 630 ~ 690 nm Near IR: 760 ~ 900 nm
Image size	Pan: 11,600 rows × 12,076 columns MS: 2,900 rows × 3,019 columns

4. Digital elevation model

A digital elevation model, produced by using photogrammetric procedures, with a ground resolution of 4 m was used in this study. Figure 1 depicts the shaded relief of the study area computed from the digital elevation model assuming an azimuth of 315° and an altitude of 45° as the position of the illumination source.

5. Ancillary data

In addition to aerial photographs and satellite images, this study used topographic maps (1:1000), orthoimages (1:5000), land cover maps, ground control points (GCP) measured using real-time kinematic (RTK) GPS, and field data to evaluate the quality of the lidar dataset. For photogrammetric processes, ground control points were measured using high-precision survey instruments such as GPS and total stations.

METHODS

1. Processing of the DEM and ancillary data

The DEM was in the ARC/INFO GRID

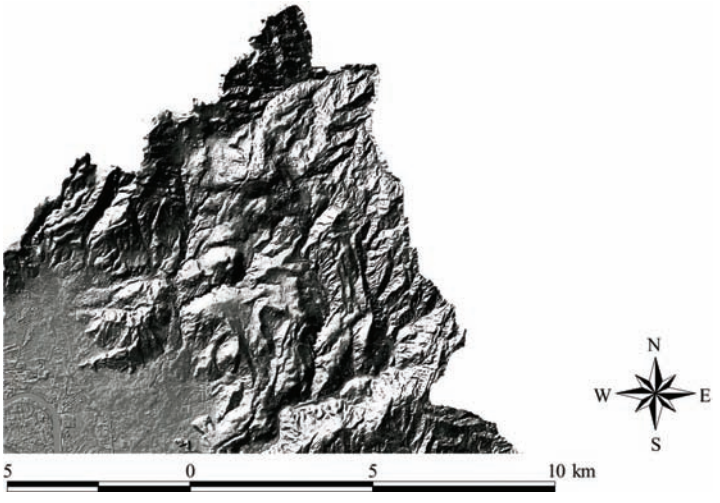

Fig. 1. Shaded relief of the study area produced from the DEM.

format with a cell size of 4 m. Originally, the values of DEM cells were orthometric height, i.e., elevation above the geoid, an equipotential gravitational surface located approximately at mean sea level (Wolf and Ghilani 2002), and the coordinate system was TWD67 (Taiwan geodetic datum based on the Geodetic Reference System 1967, GRS67) (Yang et al. 2001). Elevation values of the lidar dataset were the geodetic height (or geometric height, the height above a reference ellipsoid), and the coordinate system was WGS84 (World Geodetic System 1984), which is similar to TWD97 (Taiwan geodetic datum based on the Geodetic Reference System 1980, GRS80) (Yang et al. 2001). Table 4 shows the parameters that define the GRS67, GRS80 and WGS84 ellipsoids, which are mathematical surfaces selected to give a good fit of the ellipsoid to the geoid over a large area (Wolf and Ghilani 2002). Illustration of the ellipsoid and geoid is shown in Fig. 2. In order to perform comparisons with the lidar data, the geoidal undulation (the vertical distance between the ellipsoid and geoid) of each DEM cell was calculated using a computer program provided by the Ministry of the Interior, Executive Yuan, Taiwan, and subsequently the DEM was transformed to TWD97 with elevations representing geodetic height. The relationship between orthometric height and geodetic height is given by the equation: $H = h - N$, where N is the geoidal undulation, and H and h are the orthometric and geodetic heights, respectively (Fotopoulos et al. 2003).

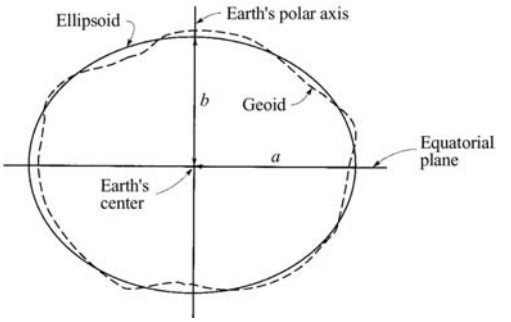

Fig. 2. Ellipsoid and geoid (Wolf and Ghilani 2002).

In addition to the DEM, all the other ancillary data, including various vector and raster maps, were transformed to TWD97 such that they could be overlaid with the DEM and the lidar data. The DEM was used as the reference for the ground elevation model, with which the ground elevation model produced resulting from the lidar data was compared. To convert the coordinate system of various thematic maps from TWD67 to TWD97, software programs written in C programming language and ARC/INFO AML (Arc Macro Language) were developed for this study.

2. Processing of the satellite images

The satellite images were QuickBird standard imageries bundled with both panchromatic and multispectral images in GeoTIFF format. Processed by the vendor, the standard imagery was normalized for topographic relief with respect to the reference ellipsoid using a coarse DEM. However, only minimal normalization was done, and for

Table 4. Defining parameters for the GRS67, GRS80, and WGS84 ellipsoids

Ellipsoid	Semiaxis a (m)	Semiaxis b (m)	Flattening f
GRS67	6,378,160.0000	6,356,774.5161	1/298.247167427
GRS80	6,378,137.0000	6,356,752.3141	1/298.257222101
WGS84	6,378,137.0000	6,356,752.3142	1/298.257223563

high-relief areas, terrain corrections must be applied in order to achieve better accuracy (DigitalGlobe, 2004). The coordinate system of the images was UTM zone 51. In order to share a common coordinate system with the other data, by the use of PCI Geomatica OrthoEngine, the images were orthorectified using ground control points obtained from the orthoimages and topographic maps.

3. Processing of the aerial photos

Digital photogrammetric procedures were applied to process the aerial photos in order to generate a digital surface model (AP DSM) for the study area. This study used ImageStation Stereo Softcopy Kits (SSK) from Z/I Imaging (Huntsville, Alabama, U.S.A.) for photogrammetry. Figure 3 depicts the workflow of the digital photogrammetric procedures. To obtain accurate geometric and imaging details, the films of the aerial photographs were scanned and converted into digital format using a photogrammetric quality scanner. The pixel resolution was 21 μm, or approximately 1,200 dpi (dots per inch). For aerial triangulation, ground control points used in the photogrammetric process were measured using the RTK GPS survey procedure.

4. Processing of the lidar data

Lidar datasets contain irregularly spaced points with 4 measurement readings, i.e., easting, northing, elevation, and intensity of the returned pulse. As shown in Table 1, this study used 3 datasets which included all points, surface points, and ground points. The data were text files, and the (X, Y, Z) values were in the TWD97 coordinate system with elevation representing geodetic height. In order to make comparisons with the DEM, the datasets were converted to ARC/INFO raster grids with a common origin and cell size with

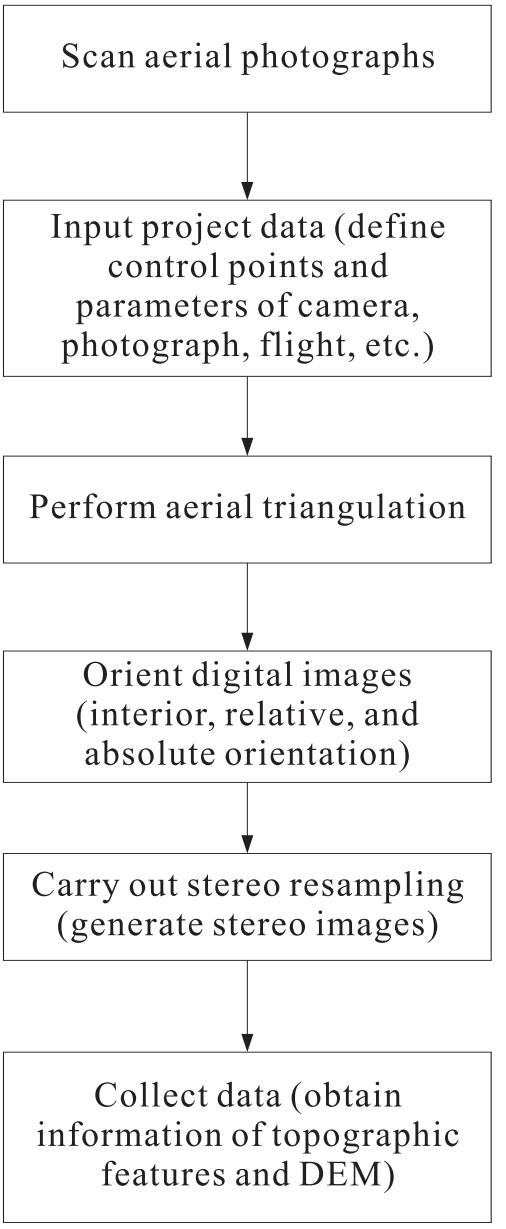

Fig. 3. Workflow of the digital photogrammetric procedures.

the DEM. From the dataset containing all data points, the minimum elevation, maximum elevation, average elevation, and number of points within each grid cell were computed, and the corresponding GRID maps were created. Moreover, the lidar datasets were

converted into vector maps, i.e., ARC/INFO point coverages. All data conversions were done using software programs written in C programming language and AML.

The lidar digital surface model (LIDAR DSM) was defined as the elevation model containing maximum elevation values. The lidar canopy height model (LIDAR CHM) was obtained by subtracting the DEM from the LIDAR DSM. Processing of the lidar data required a large amount of computer disk space and memory because the size of the original data was quite large. To reduce processing time, a subset of the lidar dataset, 1×1 km, was selected to experiment with the analytical methods developed for this study.

RESULTS

1. Orthorectified satellite images

In order to orthorectify the QuickBird images, orthoimages (produced from aerial photos), topographic maps, and the 4-m DEM were used in the geometric correction process. In total, 9 ground control points were selected for georeferencing, and the root mean square errors (RMSEs) for these control points were 1.56 and 0.39 m for the panchromatic and multispectral images, respectively. Table 5 shows the residuals for the control points. It was observed that due to the rugged terrain and dense vegetation, it was difficult to locate ideal ground control points in the image. Choosing more control points did not necessarily reduce the RMSE, because the added points possibly introduced additional displacement errors into the coordinate transformation computation. Figure 4 depicts the orthorectified multispectral image acquired for this study.

Laser scanning provides highly accurate positional measurements comparable to photogrammetric measurements (Baltsavias 1999). For accuracy assessment and characterization of various surface features that reflect laser pulses, a high accuracy level of ancillary data is required. According to the mapping standard, the horizontal and vertical accuracies of the 1:1000 topographic maps are within 0.2 and 1 m, respectively. The accuracy value for the 4-m DEM is 0.5 m for flat areas, and 1.4 m for mountainous areas except under a closed canopy. Associated with the topographic maps and DEM, the

Table 5. Root mean square error and residuals for the ground control points obtained from the QuickBird satellite images

Control point ID	Multispectral image			Panchromatic image		
	Residual	Residual X	Residual Y	Residual	Residual X	Residual Y
1	0.63	0.03	0.63	2.54	0.11	2.54
2	0.58	-0.17	-0.55	2.32	-0.67	-2.22
3	0.47	-0.09	-0.46	1.87	-0.37	-1.83
4	0.37	0.10	0.35	1.46	0.39	1.41
5	0.29	0.07	-0.28	1.14	0.28	-1.11
6	0.16	0.07	0.15	0.66	0.29	0.59
7	0.11	-0.03	0.10	0.43	-0.11	0.42
8	0.09	0.05	0.08	0.37	0.21	0.30
9	0.02	0.00	-0.02	0.10	0.01	-0.10
RMSE	0.39	0.09	0.38	1.56	0.35	1.52

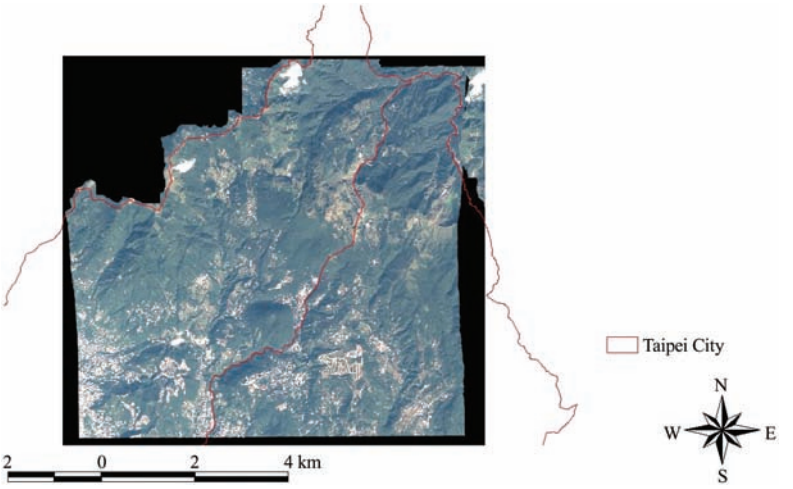

Fig. 4. Orthorectified QuickBird multispectral image.

orthorectified satellite images provided valuable information for interpretation of land cover types in the study area.

2. DSM generated from the aerial photos

Figure 5 shows one of the aerial photos acquired for this study. The photos were recorded on 23×23 cm large-format color film. With 21-μm pixel resolution (46.2-cm ground resolution), each digital image file required about 367 MB of storage space. The overlap of 2 adjacent photos in the same flight line was about 75%. As compared to the multispectral image, the aerial photos provided more detailed information about the ground surface due to their higher spatial resolution.

To increase viewing performance during the photogrammetric processes, image pyramids for different scales were produced from the original images. After collecting measurements of carefully selected ground points appearing on overlapping images, stereo models were created for the study area by performing stereo resampling on the image pairs. When needed, information on topographic features was collected directly from the images using photogrammetric tools provided by ImageStation. For rugged surfaces such as that which exists in the study area, digital photogrammetric techniques provide accurate measurements much more efficiently than traditional field surveys. To compare with the LIDAR DSM, an AP DSM with 4-m resolution was generated by an automatic matching technique. The (X, Y, Z) data of the AP DSM were then converted into an ARC/INFO grid map using a C language

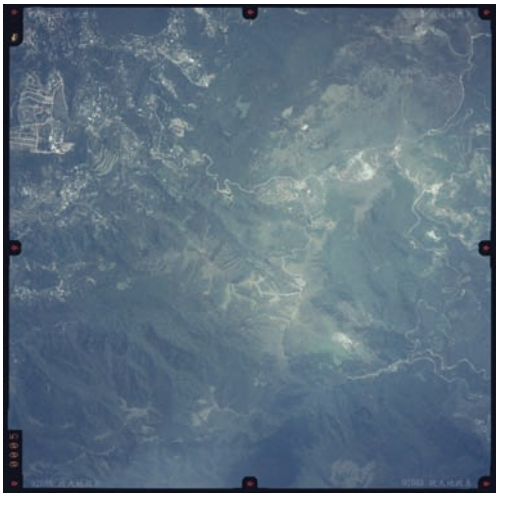

Fig. 5. Aerial photo.

program. Figure 6 shows the DSM generated from the aerial photos.

3. Observations from the lidar data

The data points were collected using an across-track scanning pattern, with a density of approximately 0.62 points/m^2. The raw data were converted to an ARC/INFO raster grid with a 4-m cell size. The entire lidar dataset and the location of the experimental site for further analysis are shown in Fig. 7. As shown in that figure, a large portion of the study area had no lidar data due to clouds in the area at the time of data acquisition. As a result of applying a filtering process to the raw data, the surface points dataset and the ground points dataset were also provided by the vendor.

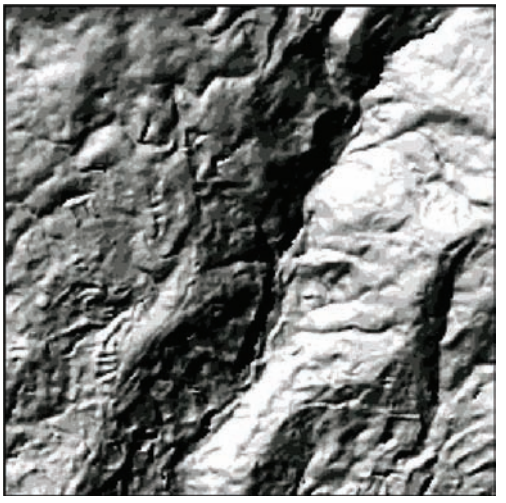

Fig. 6. Digital surface model produced using aerial photos.

Two types of maps were produced from the lidar datasets, i.e., ARC/INFO point coverages and raster grids. Figure 8 depicts the lidar data classified as surface and ground points overlaid on top of the panchromatic satellite image. As shown in Fig. 8, the number of surface points was much greater than of ground points. Figure 9 shows a close-up look of these points. The lidar sensor collects data by scanning objects on the ground in a direction perpendicular to the flight direction. Measurements of these points showed that the horizontal distance between adjacent points on the same scan line were mostly less than 2 m, with very few of them

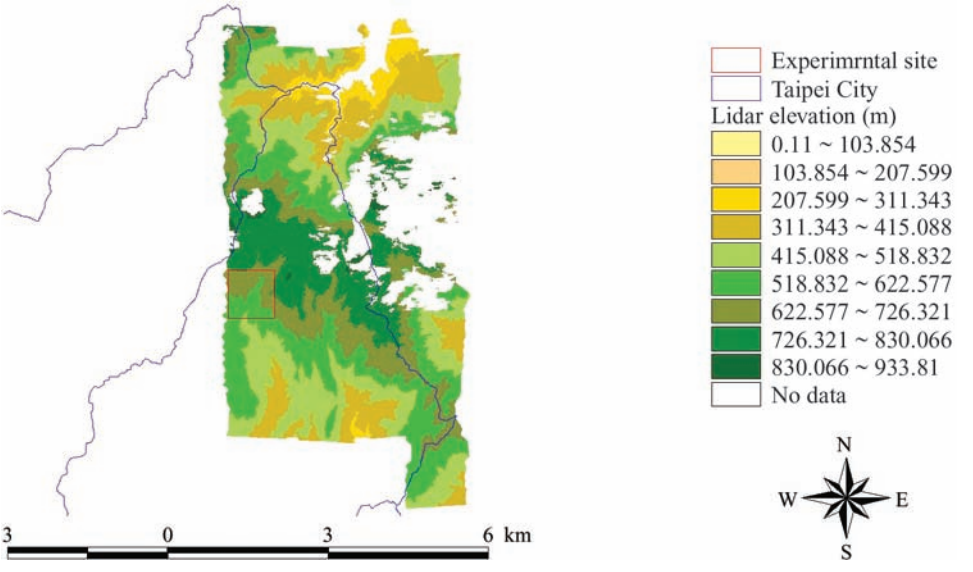

Fig. 7. Lidar data and the experimental site.

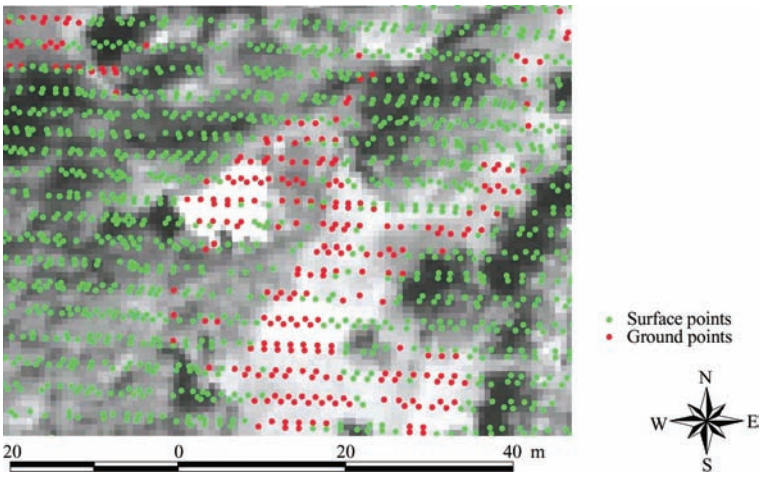

Fig. 8. Satellite image overlaid with points classified as surface and ground points.

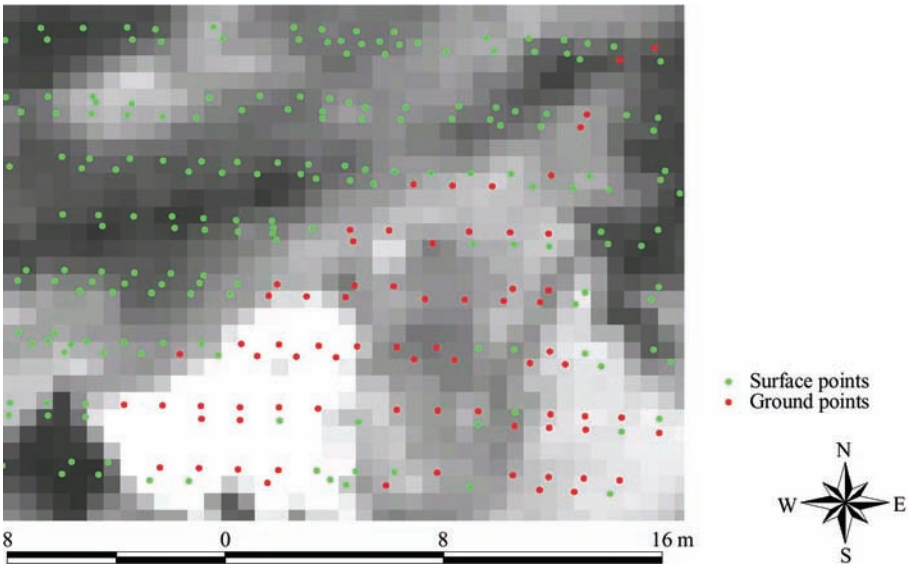

Fig. 9. Close-up look of lidar data points.

separated by more than 3 m. Along the flight direction, 2 adjacent scan lines were spaced at about 1 m, followed by another pair of scan lines about 2 m apart from the previous scan line.

The lidar data points were grouped into 4×4-m grid cells, and within each cell, statistical analysis was performed. Because of the high point density, only very few grid cells were voids, i.e., with no observation of lidar pulses. For the 1×1-km experimental site, only 15 of 62,500 cells were voids, which amounted to 0.024% of the experimental area. All other cells had at least 1 data point, with a maximum of 166 points. Figure 10 depicts the histogram of the number of data points in the grid cells. The statistics showed that 59.87% of the

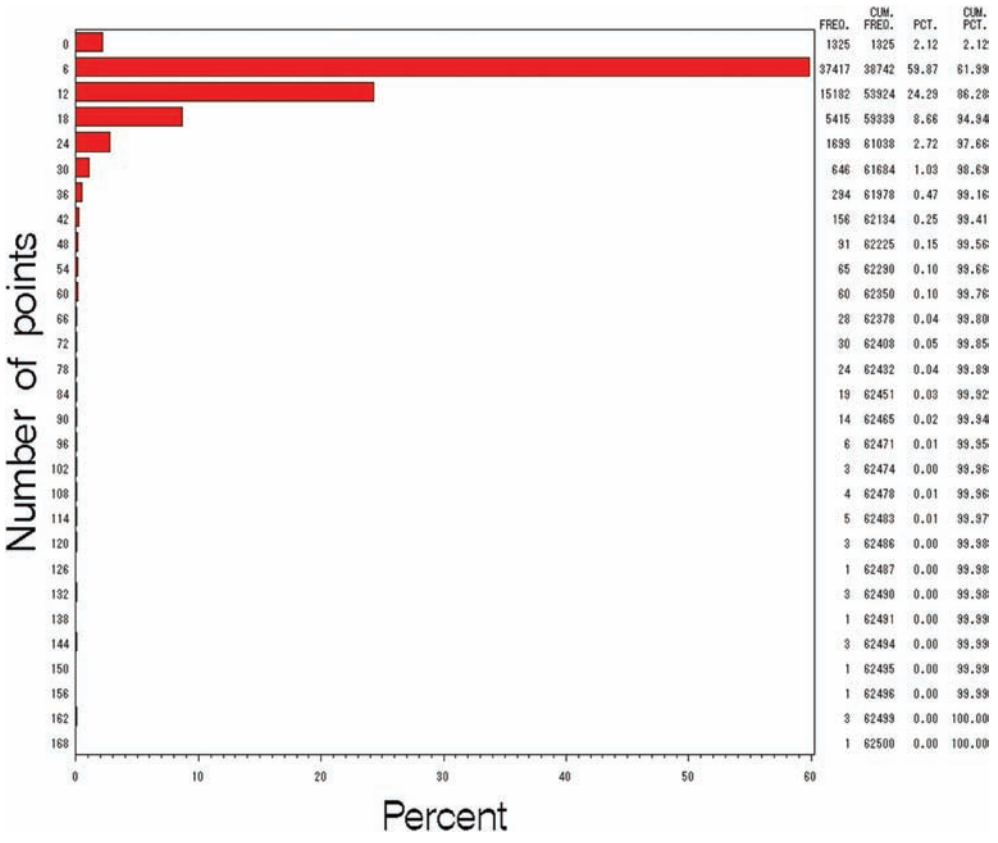

Fig. 10. Histogram of the number of data points in 4×4-m grid cells.

grid cells had between 3 and 8 data points. Those cells having a large number of data points appeared to be in areas that overlapped between flight lines. For those cells with no hits, a close-up examination found that these cells were located in shaded areas obstructed by buildings or other structures.

4. Estimation of canopy height

As shown in Figs. 8 and 9, the data points classified as ground points and surface points did not cover the entire study area. However, estimation of canopy surface elevation and ground elevation are both needed for each grid cell in order to estimate the canopy height. Figure 11 shows the multispectral satellite image of the 1×1-km experimental site overlaid with all ground points. Close examination showed that the ground points mostly appeared in roads, structures, and areas with sparse vegetation,

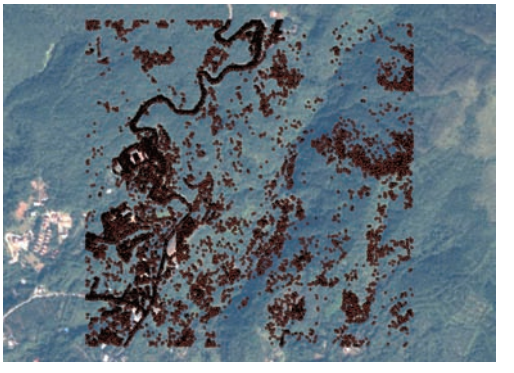

Fig. 11. Satellite image of the 1×1-km experimental site overlaid with lidar ground points.

and only a small number of them appeared in densely vegetated areas. Due to insufficient coverage of ground points, it was difficult to derive an accurate estimation of a ground elevation model using the ground points alone. Therefore, this study derived the LIDAR DSM from the dataset containing data of all points, and directly utilized 4-meter DEM as the ground elevation model.

To evaluate the quality of the DEM, the (X,Y) coordinates of 27 ground control points measured using RTK GPS and the lidar ground points were used to compute surface elevations by interpolating from a triangulated irregular network (TIN) created using the DEM. In addition, a TIN was created from the lidar ground points for comparison between the GCPs and the lidar data. Table 6 summarizes the comparisons of the elevations of GCPs, lidar ground points, and the DEM.

The canopy height model (CHM) was represented by the difference between the DSM and DEM. Analyzed on a per cell basis, the LIDAR DSM represented by the maximum value is shown in Fig. 12. The CHMs derived from processing of the lidar data and the aerial photos are shown in Figures 13 and 14, respectively.

Table 6. Comparisons of elevations of GCPs, lidar ground points, and the DEM

Variable	Number of observations	Mean (m)	Maximum (m)	Minimum (m)	Standard deviation (m)
$G_h - D_h$	27	0.4121	1.8735	-1.6612	0.9214
$G_h - L_t$	27	1.5000	2.2988	-2.5522	0.9357
$L_h - D_h$	23157	-0.4446	15.4341	-15.9124	2.3765

[1)] G_h, elevation of the ground control point; D_h, elevation computed by interpolating from the TIN created using the DEM; L_t, elevation computed by interpolating from the TIN created using the lidar ground points; L_h, elevation of the lidar ground point.

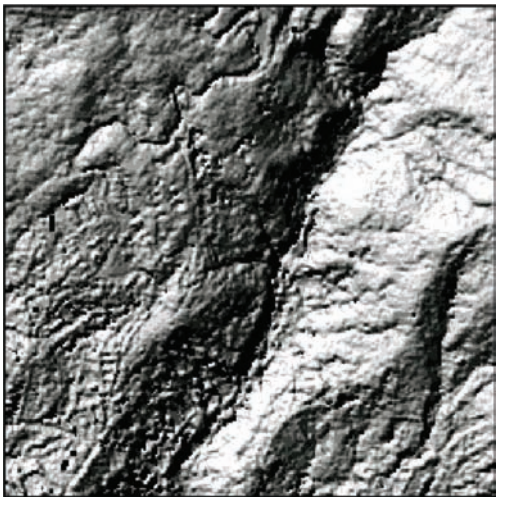

Fig. 12. Canopy surface model produced using the lidar data.

Fig. 13. Canopy height model derived from the lidar data.

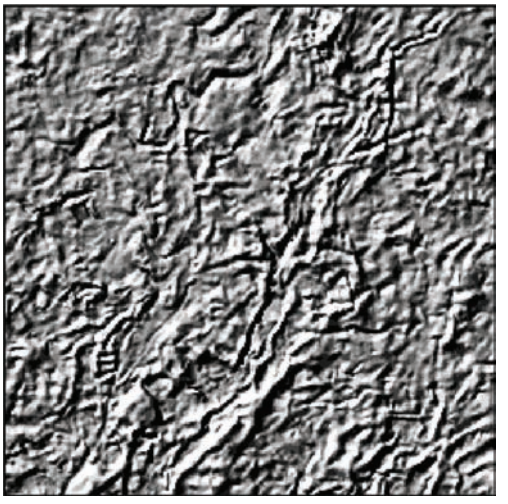

Fig. 14. Canopy height model derived from the aerial photos.

DISCUSSION

As shown in Table 6, the differences between elevations interpolated from the TIN created using DEM and the corresponding elevations of GCPs ranged from -1.66 to 1.87 m, with a mean difference of 0.41 m, and a standard deviation of 0.92 m. When comparing elevations of the lidar ground points with corresponding GCPs and the DEM, larger variations were observed, and the mean difference were 1.5 and -0.44 m, respectively. The accuracy of lidar measurements is highly dependent on the terrain slope, surface roughness, and land cover (Kraus and Pfeifer 1998, Baltsavias 1999). Further study is needed to evaluate the accuracy of the lidar ground points used herein.

Accurate estimation of the CHM requires a good-quality DEM. For mountainous areas such as the experimental site, the 4-m DEM used in this study should be suitable for estimation of the CHM. Kraus and Pfeifer (1998) indicated that laser scanner data provide DEMs in wooded areas with an accuracy equivalent to photogrammetric DEMs. Various algorithms for determining DEM from the lidar data will be explored in the future.

By comparing Figs. 6 and 12, one can see that the variation in the LIDAR DSM is larger than that of the AP DSM. This was because the AP DSM was produced by interpolating the stereo image model during the automatic matching process; in contrast, the LIDAR DSM was generated from the local maximum in each grid cell.

As shown in Figs. 13 and 14, it appears that the LIDAR CHM has much greater detail than the AP CHM. In comparison, the shaded relief image of the LIDAR CHM has greater similarity to the aerial photos and satellite images as compared to that of the AP CHM.

A paired *t*-test was performed on the CHMs produced both from the lidar data and aerial photos. The statistical results show that the mean difference between the LIDAR CHM and the AP CHM was 0.22 m with a standard deviation of 2.59 m, and the canopy height derived from the lidar data was larger than that derived from the aerial photos ($p < 0.0001$). This difference may have resulted from the methods used to generate the canopy surface models from these 2 types of data.

CONCLUSIONS

While a more-complete analysis is needed to evaluate the accuracy of estimation of forest canopy height, the results indicate that lidar data have great potential for directly measuring forest canopy structures. Further study will focus on validation of the predicted lidar canopy height with field survey data, and methodologies for determining DEM with lidar data and integrating remote sensing data with lidar data to improve the accuracy

of classification results as well as canopy height estimations.

ACKNOWLEDGEMENTS

The author would like to thank the Agricultural and Forestry Aerial Survey Institute, Taipei, Taiwan for providing data, and the National Science Council of the R.O.C. for providing support (NSC92–2313–B–004 –001) for this study. My gratitude also goes to the Council of Agriculture, Taipei, Taiwan, and Prof. Shih of National Chiao Tung University, Hsinchu, Taiwan for sponsoring and supervising the lidar pilot project, which resulted in data for this study.

LITERATURE CITED

Anonymous. 2004. Looking to the future. Available at Taipei, Taiwan: Yangmingshan National Park Headquarters, Ministry of the Interior, Executive Yuan. http://www.ymsnp.gov.tw/HTML/ENGNEW/info/information.htm (accessed 28 April 2004).

Baltsavias EP. 1999. A comparison between photogrammetry and laser scanning. ISPRS J Photogram Remote Sens 54:83-94.

Brown de Colstoun EC, Story MH, Thompson C, Commisso K, Smith TG, Irons JR. 2003. National park vegetation mapping using multi-temporal Landsat 7 data and a decision tree classifier. Remote Sens Environ 85:316-27.

DigitalGlobe. 2004. QuickBird Imagery Products–Prouduct Guide. Longmont, CO: DigitalGlobe, Inc. p 13-26.

Drake JB, Dubayah RO, Clark DB, Knox RG, Blair JB, Hofton MA, Chazdon RL, Weishampel JF, Prince SD. 2002. Estimation of tropical forest structural characteristics using large-footpring LIDAR. Remote Sens Environ 79:305-19.

Fassnacht KS, Gower ST, MacKenzie MD, Nordheim EV, Lillesand TM. 1997. Estimating the leaf area index of north central Wisconsin forests using the Landsat thematic mapper. Remote Sens Environ 61:229-45.

Fotopoulos G, Kotsakis C, Sideris MG. 2003. How accurately can we determine orthometric height differences from GPS and geoid data? J Surv Eng 129(1):1-10.

Franklin SE. 2001. Forest change detection. In: Remote sensing for sustainable forest management. New York: Lewis Publishers. p 287-320.

Haara A, Haarala M. 2002. Tree species classification using semi-automatic delineation of trees on aerial images. Scand J For Res 17:556-65.

Hudak AT, Lefsky MA, Cohen WB, Berterretche M. 2002. Integration of lidar and Landsat ETM+ data for estimating and mapping forest canopy height. Remote Sens Environ 82:397-416.

Imhoff ML, Sisk TD, Milne A, Morgan G, Orr T. 1997. Remotely sensed indicators of habitat heterogeneity: use of synthetic aperture radar in mapping vegetation structure and bird habitat. Remote Sens Environ 60:217-27.

Kraus K, Pfeifer N. 1998. Determination of terrain models in wooded areas with airborne laser scanner data. ISPRS J Photogram Remote Sens 53:193-203.

Lefsky MA, Harding D, Cohen WB, Parker G, Shugart HH. 1999. Surface lidar remote sensing of basal area and biomass in deciduous forests of eastern Maryland, U.S.A. Remote Sens Environ 67:83-98.

Lefsky MA, Cohen WB, Parker GG, Harding DJ. 2002. Lidar remote sensing for ecosystem studies. Bioscience 52(1):19-30.

Leica Geosystems. 2002. ALS40 airborne laser scanner product description. Atlanta, GA: Leica Geosystems. p 1-10.

Lim K, Treitz P. 2002. Estimating above-ground biomass using lidar remote sensing. In:

Remote Sensing for Agriculture, Ecosystems, and Hydrology IV Conference. Proceeding of SPIE's International Symposium on Remote Sensing; 2002 Sept 23-27; Agia Pelagia, Crete, Greece: Society Photo-Optical Instrumentation Engineers.

Lim K, Treitz P, Wulder M, St-Onge B, Flood M. 2003. Lidar remote sensing of forest structure. Progr Phys Geogr 27(1):88-106.

Skakun RS, Wulder MA, Franklin SE. 2003. Sensitivity of the thematic mapper enhanced wetness difference index to detect mountain pine beetle red-attack damage. Remote Sens Environ 86:433-43.

Ulbricht KA, Heckendorff WD. 1998. Satellite images for recognition of landscape and landuse changes. ISPRS J Photogram Remote Sens 53:235-43.

Utkin AB, Lavrov AV, Costa L, Simoes F, Vilar R. 2002. Detection of small forest fires by lidar. Appl Phys B 74:77-83.

Viedma O, Melia J, Segarra D, Carcia-Haro J. 1997. Modeling rates of ecosystem recovery after fires by using Landsat TM data. Remote Sens Environ 61:383-98.

Wehr A, Lohr U. 1999. Airborne laser scanning–an introduction and overview. ISPRS J Photogram Remote Sens 54:68-82.

Wolf PR, Ghilani CD. 2002. Elementary surveying: an introduction to geomatics, 10th ed. Upper Saddle River, NJ: Prentice Hall. p 540-1.

Wulder MA. 1998. The prediction of leaf area index from forest polygons decomposed through the integration of remote rensing, GIS, UNIX, and C. Comput Geosci 24:151-7.

Wulder MA, Kurz WA, Gillis M. 2004. National level forest monitoring and modeling in Canada. Progr Plann 61:365-81.

Yang M, Tseng CL, Yu JY. 2001. Establishment and maintenance of Taiwan geodetic datum 1997. J Surv Eng 127(4):119-32.